J. Biochem. 2010;147(1):95–107 doi:10.1093/jb/mvp152

JB THE JOURNAL OF BIOCHEMISTRY

Structure and reaction mechanism of human nicotinamide phosphoribosyltransferase

Received August 26, 2009; accepted September 2, 2009; published online October 9, 2009

Ryo Takahashi[1], Shota Nakamura[1], Takashi Nakazawa[2], Katsuhiko Minoura[3], Takuya Yoshida[1], Yoshinori Nishi[3], Yuji Kobayashi[3,*] and Tadayasu Ohkubo[1]

[1]Graduate School of Pharmaceutical Sciences, Osaka University, Suita, Osaka 565-0871; [2]Department of Chemistry, Nara Women's University, Nara 630-8506 and [3]Osaka University of Pharmaceutical Sciences, Takatsuki, Osaka 569-1094, Japan

*Yuji Kobayashi, Osaka University of Pharmaceutical Sciences, Takatsuki, Osaka 569-1094, Japan, Tel/Fax: +81 72 690 1080, E-mail: kobayasi@gly.oups.ac.jp

Nicotinamide (NM) phosphoribosyltransferase (NMPRTase) catalyzes the reaction of NM and 5′-phosphoribosyl-1′-pyrophosphate (PRPP) to form NM mononucleotide (NMN) and pyrophosphate (PPi) in the pathway of NAD-biosynthesis. Monitoring the ^{1}H and ^{31}P NMR spectra of the reaction mixture, we found that this reaction is reversible as dictated by the equilibrium constant $K = [NMN][PPi]/([NM][PRPP]) = 0.14$, which agreed well with the ratio of second-order rate constants for forward and backward reactions, $K = 0.16$. The crystal structures of this enzyme in the free form and bound to NM and PRPP at the resolution of 2.0–2.2 Å were essentially identical to that of the complex with NMN, except for some variations that could facilitate the substitution reaction by fixing the nucleophile and the leaving group for the requisite inversion of configuration at the C1' carbon of the ribose ring. In the active site near the C1' atom of the bound PRPP or NMN, there was neither negatively charged group nor waterproof environment necessary to support the feasibility of a ribo-oxocarbocation intermediate inherent in the S_N1 mechanism. The structures and catalytic mechanism thus revealed are also discussed in connection with the multiple biological functions of NMPRTase.

Keywords: chemical equilibrium/multi-functional enzyme/nicotinamide phosphoribosyltransferase/S_N2/visfatin/X-ray analysis.

Abbreviations: KIE, kinetic isotope effect; NM, nicotinamide; NMN, nicotinamide mononucleotide; NMPRTase, nicotinamide phosphoribosyltransferase; PDB, Protein Data Bank; 5PR-1,2-CP, 5-phosphoribosyl cyclic-1,2-phosphate; PRPP, 5′-phosphoribosyl-1′-pyrophosphate; R-1,5-CP, ribose cyclic-1,5-phosphate.

Nicotinamide (NM) phosphoribosyltransferase (NMPRTase) catalyzes the synthesis of NM mononucleotide (NMN) from NM and 5′-phosphoribosyl-1′-pyrophosphate (PRPP) in the NAD biosynthesis pathway, as shown in Fig. 1 (*1*, *2*). The resulting NAD plays essential roles as a co-enzyme in a large number of redox reactions, energy metabolism and anabolic/catabolic pathways (*3*). NAD also serves as a substrate, which is degraded to NM and cyclic ADP-ribose by ADP-ribosyl cyclase in signal transduction, and is used in the enzyme regulation by ADP-ribosylation (*4*, *5*). Proper physiological levels of NAD are maintained by biosynthesis utilizing either NMN or nicotinic acid (NA) mononucleotide (NAMN) as precursors. NA phosphoribosyltransferase (NAPRTase) and quinolinic acid (QA) phosphoribosyltransferase (QAPRTase) are responsible for the *de novo* synthesis of NAMN from NA and QA, respectively.

A remarkable feature of these NAD synthetic pathways is that NM can be reused in two ways: (i) NM is successively converted to NA and NAMN (ii) NM is converted to NMN and then to NAD. However, route (i) is not available in humans because NM deaminase activity occurs only in people infected with the malarial parasite (*6*). Inhibitors of NMPRTase, which cause exhaustion of NAD and disorder of NAD-requiring systems of mitochondrial respiratory and energy metabolism, should be candidates for new anti-cancer drugs like FK866 (*7*, *8*). It is therefore expected that new and more potent anti-cancer drugs could be developed by the rational design of an inhibitor based on the structure and reaction mechanism of NMPRTase.

NMPRTase was once called pre-B cell colony-enhancing factor (PBEF) because it was originally identified as a growth factor for early stage B cells (*9*, *10*). The identity of this enzyme as a cytokine secreted by visceral fat tissues has been a controversial issue associated with its binding to and activation of the insulin receptor (*11–14*). There is still no consensus on the relationship among a wide variety of functions exerted by a single enzyme, NMPRTase (PBEF or visfatin), even after the X-ray structures of NMPRTase in free and product- or inhibitor-bound forms have been solved. These structures include 2GVL (murine, free), 2H3D (murine, complex with NMN), 2GVG (human, complex with NMN), 2GVJ (human, complex with FK866), 2G95 (rat, free), 2G96 (rat, complex with NMN) and 2G97 (rat, complex with FK866) deposited in PDB (*15–17*). We corroborated the X-ray data 2E5B (human, free state), 2E5D (human, complex with NM) and 2E5C (human, complex with PRPP) to cover the whole stages of the enzyme reaction from the binding with the substrate,

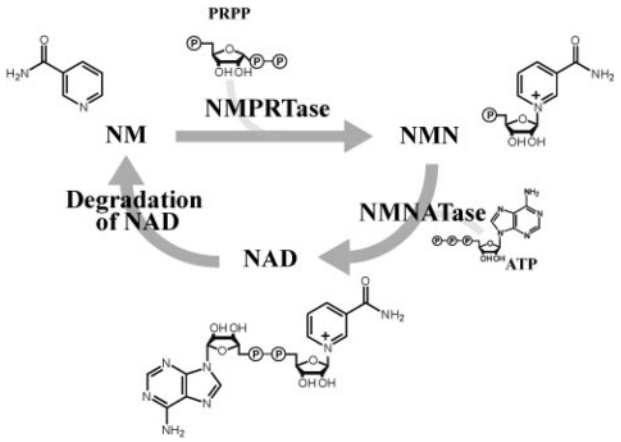

Fig. 1 Cyclic metabolic pathway of NAD biosynthesis from NM and recycle of NM from NAD in cells. ATP is required for the synthesis of NAD from NMN.

formation of a transition state (if any), and the release of products (*18*). Despite these and seminal structural studies of Schramm and co-workers (*19*, *20*), there remain considerable questions concerning the reaction mechanism of this enzyme. To design and develop possible inhibitors, a clearer and more comprehensive understanding of how the enzyme recognizes the substrate molecules and by which mechanism it catalyzes the reaction is indispensable.

Here, we report the results of investigation on the dynamic features of the reaction of NMPRTase by monitoring the concentration changes of all the reactants and products with ^{1}H and ^{31}P NMR. Kinetic analyses revealed that this catalytic reaction is described as a combination of two second-order rate constants for the formation of NMN (forward reaction) and that of PRPP (backward reaction). According to the equilibrium constant thus obtained, the backward reaction is about seven times faster than the forward reaction for the NMN synthesis. This preference of the reaction for the backward reaction has been reported in the context of chemical equilibrium, which is shown to be alterable to drive the reaction to the opposite direction by a weak coupling with the hydrolysis of ATP (*20*). Although the proposed thermodynamic model allows the enzyme to play the requisite role in the biosynthesis of NMN leading to NAD, the chemical mechanism that rationally explains the equilibrium still needs to be elaborated. It is therefore desirable to clarify the nature of the main substitution reaction before extending the study to explore the mechanism of the more complex reaction involving ATP and ADP. To compare the structures of the enzyme with respect to various binding states associated with the equilibrium, we also determined the crystal structures of human NMPRTase in its free form and two complexes with NM and PRPP in addition to those reported (*15–17*, *19*). The active-site structures of these complexes were essentially identical to those reported for the complexes with NMN. This is consistent with the reversible nature of the enzyme reaction, in which substrates and products could be recognized without appreciable conformational change. Moreover, it was found that the suggested S_N1 mechanism is unlikely because of the absence of structural and kinetic evidence supporting the existence of the ribo-oxocarbocation intermediate (we refer to this as carbocation hereafter). Based on these results, we will discuss the relationship between the structure and reaction mechanism of NMPRTase. The implication that the equilibrium state apparently disfavours the formation of NMN *in vivo* is also discussed.

Materials and methods

Expression and purification of recombinant human NMPRTase

A cDNA encoding human NMPRTase gene was cloned into *Eco*I and *Sal*I sites of the expression vector pGEX6p1 (GE Healthcare, Chalfont St Giles, UK). The plasmid was introduced into *Escherichia coli* BL21(DE3) cells for protein expression. Cultures were grown at 37°C in Luria–Bertini broth medium (*21*). When the OD_{600} reached 0.5, the cells were incubated for 3 h at 28°C with 1 mM isopropyl β-D-thiogalactopyranoside to induce the expression of the protein. Cells were harvested by centrifugation, resuspended in phosphate (Pi)-buffered saline (*21*), and broken by ultrasonication on ice. After ultracentrifugation, the soluble fraction was applied to glutathione-Sepharose resin (GE Healthcare, Chalfont St Giles, UK) and cleaved with PreScission Protease (GE Healthcare, Chalfont St Giles, UK) on column. Finally, the resulting protein was purified by gel filtration chromatography.

Circular dichroic measurement

Circular dichroic (CD) spectra of human NMPRTase were recorded at 20°C on a JASCO J-720 spectropolarimeter (Tokyo, Japan) in the range of 190–260 nm with a 1 mm path length cell. The samples for CD measurements were prepared with a protein concentration of about 130 μg/ml in 30 mM Tris–HCl buffer (pH 8.0) containing 100 mM NaCl.

Ultracentrifugation analysis

Analytical centrifugation experiments were performed on a Beckman XL-I analytical ultracentrifuge using a double-sector centerpiece and sapphire windows. The sedimentation velocity measurements were carried out at 290,000 g, 20°C and the concentration of 970 μg/ml. The sedimentation equilibrium analysis was performed at 8,000 g, 10°C, to minimize the possibility of the denaturation of the enzyme. The enzyme was dissolved in 20 mM Tris–HCl buffer (pH 8.5) containing 150 mM NaCl and 1 mM DTT at the concentrations of 240, 490 and 970 μg/ml.

Quantitative assay of recombinant NMPRTase activity

Human NMPRTase (0.1 μg) suspended in 5 μl of 20 mM Pi buffer (pH 7.5) was added to 50 μl of 5 mM Tris–HCl buffer (pH 8.5) containing 1 mM CHAPS, 2.5 mM $MgCl_2$ and 1 mM DTT. To this solution were added 1 μl of 0.5 mM ^{14}C-labelled NM and 1 μl of 2.5 mM PRPP. For the reference to the enzyme solution, 5 μl of 20 mM Pi buffer was added to 50 μl of 5 mM Tris–HCl buffer (pH 8.5). The radioactive components (including ^{14}C-labelled NMN) of the reaction mixture were analyzed on thin layer chromatography (Cellulose F 20 × 20 cm, Merck, Whitehouse Station, NJ), developed with 0.3 M aqueous LiCl solution for 2 h. The chromatogram was visualized with a radio image analyzer (BAS2000; Fuji Film, Tokyo, Japan).

^{1}H and ^{31}P NMR measurements

^{1}H and ^{31}P NMR measurements were performed at 500 MHz for ^{1}H and 200 MHz for ^{31}P on an Inova 500 (Varian, Palo Alto, CA). Two-dimensional ^{1}H-^{1}H, ^{1}H-^{31}P and ^{1}H-^{13}C NMR measurements were carried out to identify some of the reaction products. The series of 1D ^{1}H and ^{31}P NMR spectra were measured with constant time intervals to monitor the reaction process for kinetic analyses. The initial concentrations of NM and PRPP were set to 0.6 mM and

1.2 mM, respectively. In the case of the reverse reaction, the concentrations of NMN and PPi were 0.6 mM and 3 mM, respectively. The enzyme concentration was 4.3 μM in 15 mM Tris–HCl D_2O buffer at pH 8.5 containing 1 mM CHAPS, 1 mM DTT and 2.5 mM $MgCl_2$. All the NMR measurements were performed at 37°C. Curve fitting was performed by numerically solving the differential equations describing a combination of five reactions, based on the fourth-order Runge–Kutta method (*22*). The numerically integrated solutions were fitted to the observed data given in Fig. 3A together with the concentration change of PPi by the iterative least squares calculations using Nelder–Mead simplex method (*22*). We used an in-house-written program for all the calculations.

Crystallization and X-ray data collection

The crystallization experiments were carried out by the hanging drop method. Each drop consisted of 1 μl of NMPRTase solution (10 mg/ml) in the buffer (20 mM Tris–HCl, pH 8.5, 150 mM NaCl and 1 mM DTT) with 1 μl of the reservoir solution (38–40% pentaerythritol propoxylate, 50 mM Tris–HCl containing 200 mM KCl at pH 8.0–9.0). Small plate-shaped crystals of NMPRTase appeared within a week. The microseeding was carried out twice to obtain a better plate-shaped crystal (*18*).

To prepare crystals of the enzyme in complex with PRPP and NM, crystals of the free NMPRTase were soaked for 12 h at 4°C in a cryo-solution containing 45% pentaerythritol propoxylate in 200 mM KCl supplemented with either PRPP or NM (50 mM each) at pH 8.0–9.0, and then frozen by immersion in liquid nitrogen. Diffraction data were collected at the beamline BL38B1 in SPring-8 (Hyogo, Japan) in a nitrogen stream at 100 K. The data were processed using DENZO and SCALEPACK from the HKL2000 package (*23*) and further processed using the CCP4 program suite (*24*). All crystals belonged to the space group $P2_1$. The structure was solved by molecular replacement using the program MOLREP (*25*) applied to murine NMPRTase (PDB ID: 2GVL) as the search model. The data statistics are shown in Table 1.

Crystal structure determination and refinement

The initial model of human NMPRTase in the free form was subjected to maximum likelihood refinement with REFMAC (*26*). Progress of the refinement was monitored on the 3D graphics using the XtalView/Xfit program (*27*). Further refinement cycles, including automatic water molecule placement using ARP/wARP (*28*) were performed. The structure was further refined until no improvement was observed in R and R_{free}. The refined structures of NM and PRPP complexes were obtained by using the model of the free form in the same manner. Detailed refinement statistics of these three structures are summarized in Table 1. The stereochemical qualities were evaluated using the program PROCHECK (*29*). The molecular models were generated using the program PyMOL (http://pymol.sourceforge.net/). The structural coordinates have been deposited in the PDB under code 2E5B (free state), 2E5D (complex with NM) and 2E5C (complex with PRPP). Possible interactions between the enzyme and substrates were drawn schematically with the aid of LIGPLOT (*30*).

Results

Characterization of recombinant NMPRTase

We established the over-expression system of human NMPRTase in *E. coli*. The purified enzyme proved active in its ability to convert NM to NMN (data not shown). The CD measurement revealed that recombinant human NMPRTase has a helix content of ~32% in a good agreement with the values of 35–40% expected from the amino acid sequence. The apparent molecular weight was determined to be 115 kDa by the ultracentrifugation analysis, showing that NMPRTase exists as a dimer in solution. These solution properties of the dimerized enzyme were in good agreement with the results of X-ray crystallographic analysis.

Enzymatic reaction profile detected by ^1H and ^{31}P NMR measurements

The catalytic reaction of NMPRTase for the production of NMN is expressed as follows.

$$NM + PRPP \rightarrow NMN + PPi$$

Table 1. Data collection and refinement statistics.

	Free state	NM complex	PRPP complex
Data collection			
Temperature (K)	100	100	100
Space group	$P2_1$	$P2_1$	$P2_1$
Cell dimensions (Å)			
a	60.56	60.33	60.23
b	106.40	106.23	106.75
c	82.78	82.48	82.61
Resolution limits (Å)	50.0–2.0	50.0–2.0	50.0–2.2
Number of unique/observed reflections	70,989/250,483	93,034/321,804	94,136/277,989
Average redundancy	1.9	1.9	1.8
Completeness (%)	97.2	95.2	85.5
R_{merge}[a]	0.078	0.072	0.100
Refinement statistics			
Refinements resolution range (Å)	20.0–2.0	20.0–2.0	20.0–2.2
R/R_{free}[b]	0.18/0.22	0.18/0.21	0.17/0.22
RMSD from ideal			
Bonds (Å)	0.006	0.006	0.007
Angles (°)	0.933	0.939	1.007
$<B>$ for atomic model[c] (Å^2)	20.23	19.07	22.73
Ramachandran plot			
Most favored regions (%)	90.1	90.0	89.9
Additional allowed regions (%)	9.9	10.0	10.1
Generously allowed regions (%)	0.0	0.0	0.0
Disallowed regions (%)	0.0	0.0	0.0

[a] $R_{merge} = \Sigma|I_h - <I_h>|/\Sigma I_h$, where $<I_h>$ is the average intensity of reflection h and symmetry-related reflections. [b] $R = R_{free} = \Sigma||F_o|-|F_c||/\Sigma|F_o|$ calculated for reflections of the working set and test (5%) set, respectively. [c] $<B>$ is the average temperature factor for all protein atoms.

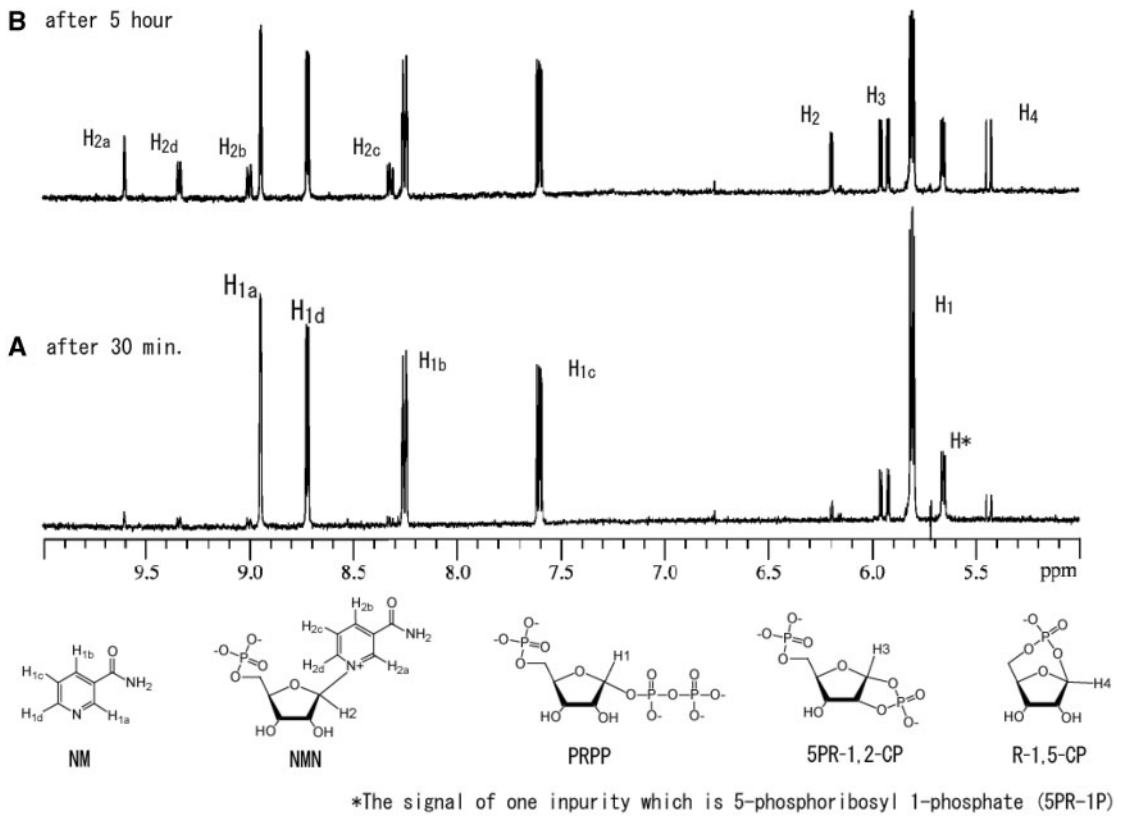

Fig. 2 Progress of the reaction catalyzed by NMPRTase as monitored by ^{1}H NMR spectra of the reactants (PRPP and NM) and the product (NMN). The spectra were recorded at 30 min (A), and at 5 h (B). Peaks were assigned as indicated by the atom labels of the corresponding structures of PRPP, NM, NMN, R-1,5-CP, 5PR-1,2-CP and PRP (5-phosphoribosyl-1-phosphate).

We initially monitored the time course of this reaction using ^{1}H NMR spectroscopy. The proton signals of pyridine rings and those of ribose C1′ were compared in Fig. 2 at an initial stage (A) and after 5 h (B). The peaks were assigned by measuring the ^{1}H NMR of authentic samples for each compound (see the label of each peak in Fig. 2). The time course of the reaction was traced by the peak intensities of each signal and plotted in Fig. 3A. As the reaction proceeds, the signal intensity of PRPP was constantly decreasing throughout the reaction, whereas that of NM to react with PRPP decreased in the beginning of the initial stage of the reaction and then slightly increased, showing a minimum at about 5 h. In contrast to the time course of NM, the initial increase in the concentration of NMN was followed by gradual decrease to a low level.

We employed ^{31}P NMR to determine the concentrations of PPi and the other phosphorus-containing compounds not detected by ^{1}H NMR. Peak areas of ^{31}P signals for these compounds could be compared with the ^{1}H signals of PRPP, which exhibits both signals, to calculate the concentrations based on the peak areas of ^{1}H signals of NM or NMN. Although it was difficult to judge the completion of the reaction or the establishment of a particular equilibrium state from the appearance of curves shown in Fig. 3A, we found that the progress of the reaction could be monitored clearly by re-plotting the data with respect to the concentrations of all the four components to obtain equilibrium constant (K) derived from the relationship $k_{2(1)}[\mathrm{PRPP}][\mathrm{NM}] = k_{2(-1)}[\mathrm{NMN}][\mathrm{PPi}]$ at the equilibrium state:

$$\mathrm{PRPP} + \mathrm{NM} \underset{k_{2(-1)}}{\overset{k_{2(1)}}{\rightleftharpoons}} \mathrm{NMN} + \mathrm{PPi} \qquad (1a)$$

$$K = \frac{k_{2(1)}}{k_{2(-1)}} = \frac{[\mathrm{NMN}][\mathrm{PPi}]}{[\mathrm{PRPP}][\mathrm{NM}]} \qquad (1b)$$

According to the plot of K versus time as shown in Fig. 3B, which allows for the value of [PPi]/[PRPP], the reaction reaches to the equilibrium at ~9 h.

We detected the signals of at least two additional compounds, which exhibited characteristic increases in concentration as the reaction proceeds. Each product was identified by ^{1}H-^{31}P heteronuclear single quantum coherence (HSQC) spectroscopy of the reaction mixture at 24 h from the start of the reaction. Referring to the known degradation products of PRPP (*31*, *32*), we identified ribose cyclic-1, 5-phosphate (R-1,5-CP) and 5-phosphoribosyl cyclic-1,2-phosphate (5PR-1,2-CP) as by-products. The furanose-ring system in R-1,5-CP was confirmed by ^{1}H-^{13}C heteronuclear multiple bond correlation (HMBC) spectrum (Supplementary Fig. S1). While the concentrations of PRPP and even the product decreased, those of 5PR-1,2-CP and R-1,5-CP increased slowly but steadily. We also observed a very slight increase in the concentration of

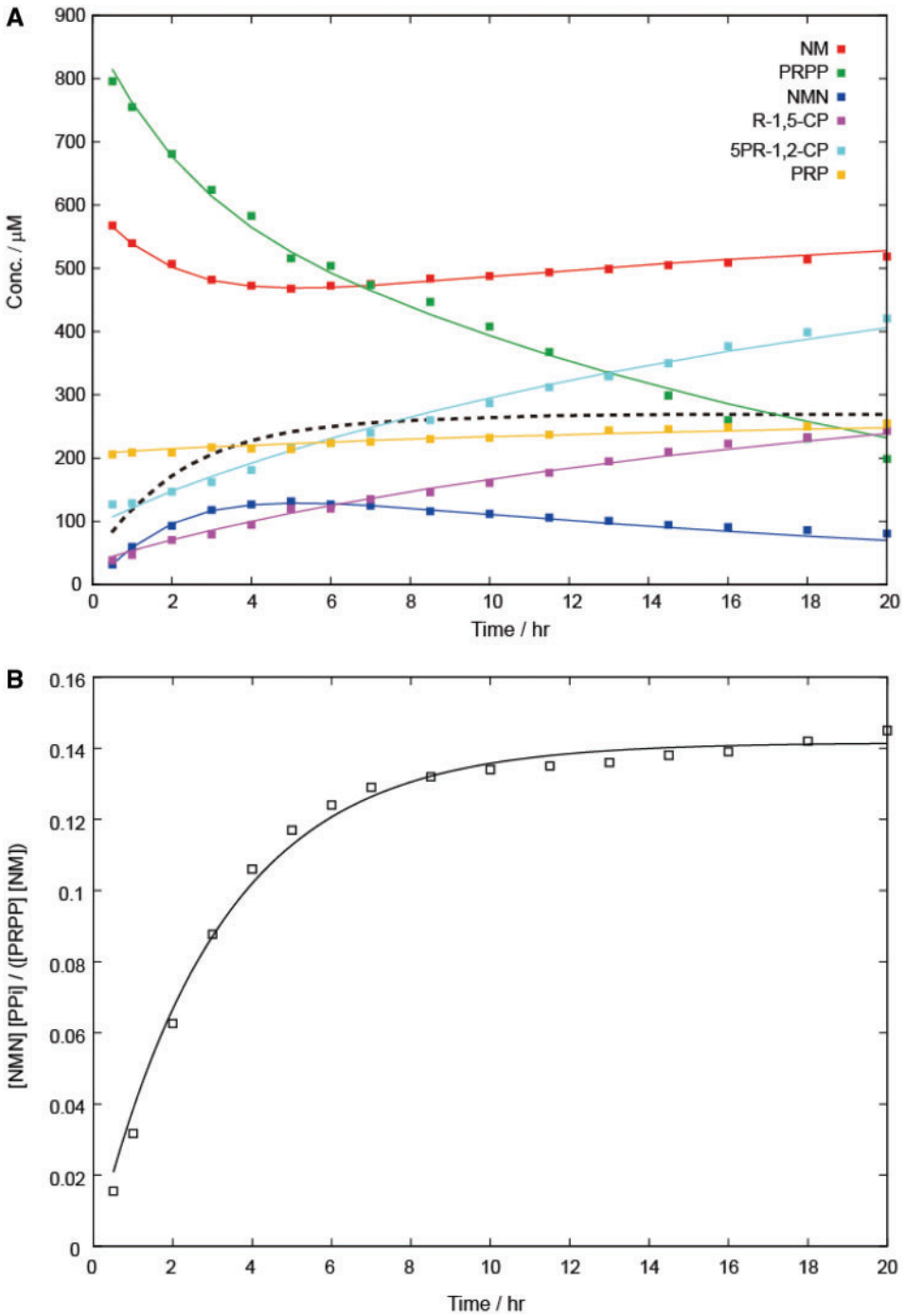

Fig. 3 Variation in the concentrations of NM (red), PRPP (green), NMN (blue), R-1,5-CP (pink), 5PR-1,2-CP (light blue) and PRP (orange) during the forward reaction. (A) The concentration of each component of the reaction mixture was determined by the intensity of ^{1}H NMR signal (Fig. 2). Solid lines were drawn by the non-linear least square fitting of data obtained from the NMR measurement. Broken line represents [PPi], which is calculated from obtained kinetic constants. (B) A plot of [NMN][PPi]/([PRPP][NM]) versus time [the same time scale as in (A)], showing the approach of the reaction to an equilibrium state represented by the equilibrium constant $K = 0.14$. The data of [PPi]/[PRPP] obtained from ^{31}P NMR measurement (Supplementary Fig. S2) were incorporated to complement ^{1}H NMR data that lack the information about [PPi]. For the plot of backward reaction, see Supplementary Fig. S4.

5-phosphoribosyl-1-phosphate (PRP), a contaminant of PRPP, probably due to the decomposition of 5PR-1,2-CP (*32*).

The reversibility of the reaction converging to an equilibrium state represented by the same equilibrium constant as measured for the forward reaction was confirmed by the experiment that starts the reaction with a mixture of NMN and PPi (Supplementary Fig. S3). To interpret these complex phenomena quantitatively, we analyzed the reaction kinetics by computational non-linear least square fitting. The best fit was obtained when the present system was assumed to be

the combination of the following reactions with the one represented by equation 1a:

$$\text{PRPP} \xrightarrow{k_{1(2)}} \text{R-1,5-CP} + \text{PPi} \quad (2)$$

$$\text{PRPP} \xrightarrow{k_{1(3)}} \text{5PR-1,2-CP} + \text{Pi} \quad (3)$$

$$\text{PPi} \xrightarrow{k_{1(4)}} 2\text{Pi} \quad (4)$$

$$\text{5PR-1,2-CP} \xrightarrow{k_{1(5)}} \text{PRP} \quad (5)$$

The numerical results including the rate constants $k_{2(1)}$, $k_{2(-1)}$, $k_{1(2)}$, $k_{1(3)}$, $k_{1(4)}$ and $k_{1(5)}$ for these reactions are summarized in Table 2.

The rate constant of the forward reaction, $k_{2(1)} = 3.9 \times 10^{-2}$/M/s, was much slower than 2.5×10^{-1}/M/s for the backward reaction $k_{2(-1)}$ in equation (1). Reflecting the dominance of the backward reaction, the position of this equilibrium is very close to the left-hand side of equation (1a) with the characteristic equilibrium constant $K = 0.14$–0.16 calculated from both the ratios of reaction rates and concentrations as given in equation (1b). Starting from NMN and PPi, the backward reaction reached nearly the same equilibrium state ($K = 0.18$) as the forward reaction, confirming that the reaction expressed by equation (1a) is indeed reversible and that both reactions are of second-order with respect to the substrate molecules (Supplementary Fig. S4). Note that the range of the value $K = 0.14$–0.18 is very close to the reported one, $K_{eq} = 0.15$ (*20*), while the assumptions and experimental conditions in these studies are quite different.

Table 2. Kinetic parameters and equilibrium constants of NMPRTase-catalyzed reaction.

Parameter[a]	
$k_{2(1)}$	3.9×10^{-2}/M/s
$k_{2(-1)}$	2.5×10^{-1}/M/s
$k_{1(2)}$	6.6×10^{-4}/s
$k_{1(3)}$	1.0×10^{-5}/s
$k_{1(4)}$	2.8×10^{-5}/s
$k_{1(5)}$	1.3×10^{-5}/s
$K = k_{2(1)}/k_{2(-1)}$	0.16
$K = \frac{[\text{NMN}][\text{PPi}]}{[\text{PRPP}][\text{NM}]}$	0.14

[a]Obtained at the enzyme concentration of 4.3 μM (pH 8.5, 37°C).

Crystal structures of NMPRTase in Free, NM- and PRPP-binding states

We determined the structure of human NMPRTase at a 2.0 Å resolution (Fig. 4A). We also obtained the crystals of complexes with the NM and PRPP substrates of the enzyme. The resolutions of the structures were 2.0 Å for the NM-complex (Fig. 4B) and 2.2 Å for the PRPP-complex (Fig. 4C). The overall structures of the free form and the complex with PRPP were very similar, with root mean square deviation of only 0.08 Å for all the Cα-atoms.

The crystal asymmetric unit contained a dimer of NMPRTase, which corresponds to the biological unit of this enzyme. The dimer exists in a head to tail configuration. The contact surface area of each monomer is ~4200 Å^2. Data collection and refinement statistics for these crystals are summarized in Table 1.

Human NMPRTase in free state was found to take the α/β barrel structure characteristic of Type II PRTase. A similar structure has also been found in NAPRTase from *Thermoplasma acidophilum* (TaNAPRTase) (*33*) and QAPRTase from *Mycobacterium tuberculosis* (MtQAPRTase) (*34*). The active site is located close to the α/β barrel on the contact surface between the monomers. The overall structures of NMPRTases of human, mouse and rat are very similar. One exception is a slight difference of loop-structure detected between human (this study) and murine (*15*) NMPRTases in free state at the region of Lys 234 – Tyr 240. However, here we will limit ourselves to focus on the structural differences in the ligand (NM, NMN and PRPP) bound state.

In the enzyme–NM complex, NM is sandwiched between the aromatic rings of Phe 193(A) and Tyr 18(B) (A or B refers to each monomer of the dimer), which are stacked one above the other (Fig. 5). Compared with the substrate-free state, these aromatic side chains relocate slightly such that both of the aromatic rings rotate about the Cβ-Cγ axis to optimally accommodate NM without changing the distance in between them (Fig. 5). The amide N7 and O7 atoms of NM can form hydrogen bonds with Asp 219(A) and Arg 311(A), respectively, allowing the ring N1 nitrogen atom to be placed at the right position to attack the ribose C1′ atom of PRPP. Probably owing to these

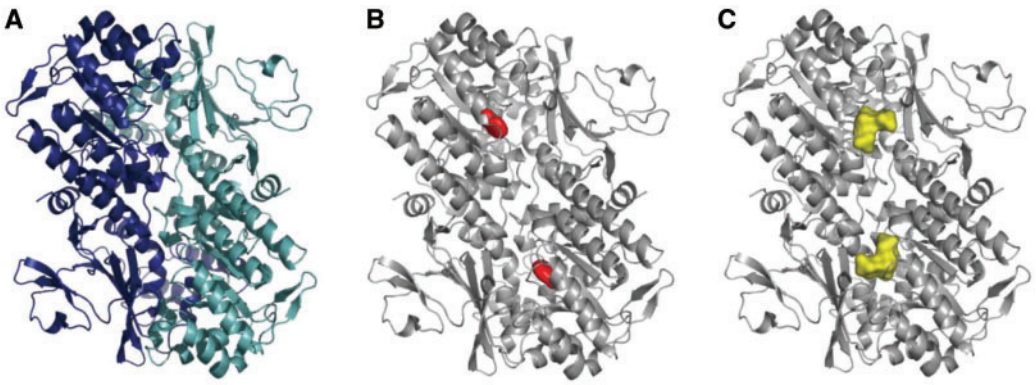

Fig. 4 The crystal structures of human NMPRTase with ribbon drawing. (A) Each monomer is distinguished by dark and light blue ribbons. (B) The complex with NM (red). (C) The complex with PRPP (yellow).

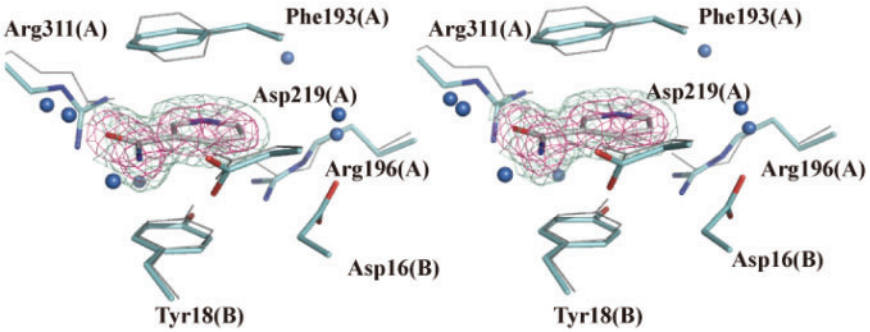

Fig. 5 Stereo view of the complex of NMPRTase with NM. The structure of the active site in the vicinity of the bound NM, which is displayed by electron density map contoured at 2.0 σ (red) and 0.7 σ (green) calculated with $2F_0-F_C$ coefficients. Several water molecules found in the vicinity of NM are illustrated with blue spheres. The change in conformation of active site residues before and after the binding with NM is shown by thin lines and solid bars, respectively. Atom labels: oxygen (red) and nitrogen (blue).

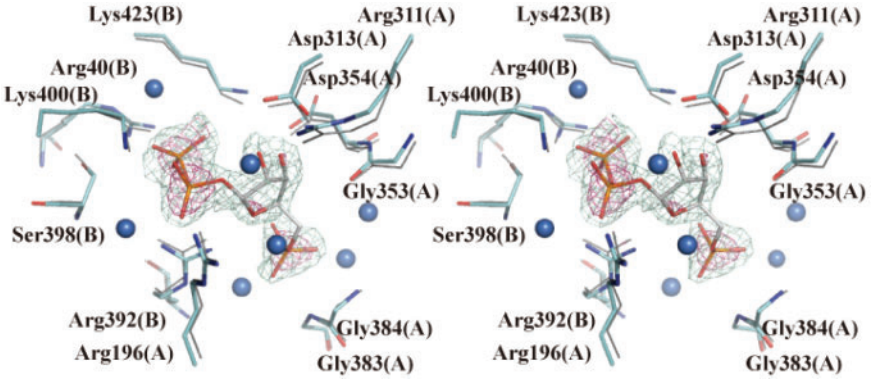

Fig. 6 Stereo view of the binding mode of PRPP in the active site. PRPP is displayed by electron density map contoured at 2.0 σ (red) and 0.7 σ (green) calculated with $2F_0-F_C$ coefficients. Several water molecules are highlighted with blue spheres as in Fig. 5. The conformational change is presented in the same manner as Fig. 5 with phosphorus atom coloured yellow.

interactions, NM occupies essentially the same site as the NM moiety of the enzyme-bound NMN (*16*) (data not shown). The active site structures are compared with respect to the free and PRPP-bound states (Fig. 6).

We could thus compare the binding modes of the sugar moieties of NMN and PRPP to the enzyme, on the grounds that the conformation of active-site residues differed very slightly and that the NM moiety of NMN (*16*) and NM almost overlapped. As shown in Fig. 7, the conformation of the ribose ring changed from the C3′-exo of PRPP to the C3′-endo of NMN. The result is that the estimated distance between the C1′ positions of their ribose moieties is 2.18 Å (Fig. 7), about half the distance of 3.82 Å between the N1 of the pyridine ring of NM and C1′ of PRPP (Fig. 8). The shift of 2.18 Å is very close to a 2.1 Å excursion of the ribosyl C1′ carbon relative to the fixed adenine ring in the corresponding reaction of adenine phosphoribosyltransferase (APRTase) from *Giardia lamblia* (*35*). Despite finding an appreciable conformational change in the ribose rings of PRPP and NMN, we were unable to detect any conspicuous distortion in their structures suggestive of the existence of the ribo-oxocarbocation intermediate. Furthermore, the observed conformational change in side-chains upon binding with PRPP may not be a large enough

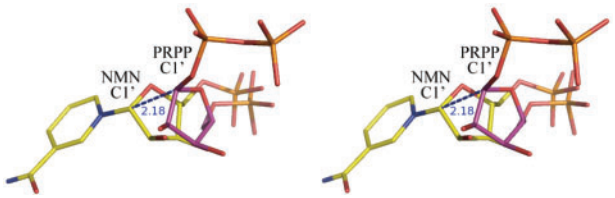

Fig. 7 Stereo view of superposed structures of PRPP and NMN in the substrate-binding site of NMPRTase. Colours of compounds and atoms are as follows: PRPP (yellow), NMN (pink), nitrogen (blue), oxygen (red) and phosphorus (orange). The enzyme-bound NM is almost completely overlapped with the NM moiety of NMN (data not shown). The distance between the C1′ carbons of PRPP and NMN is 2.18 Å as indicated by a dotted line. The C1′-N (ring nitrogen of NM) bond and C1′-O (ester oxygen of PPi) bond point to virtually the opposite directions with respect to the C1′ carbon. The co-ordinates for crystal structure of the NMN-enzyme complex were taken from PDB code 2GVG (*16*).

constraint imposed on the ribose ring to cause a highly distorted structure characteristic of the carbocation intermediate (Figs 6 and 7).

According to the comparison of structures of free and PRPP-bound enzymes (Fig. 6), we could assume several interactions between the enzyme and PRPP. The ribose moiety of PRPP is bound to the enzyme through hydrogen bonds formed by pairing O4 with NH2 of Arg 392(B), O2 with NH1 of Arg 311(A), O2 with OD2 of Asp 313(A) and O3 with OD1 of

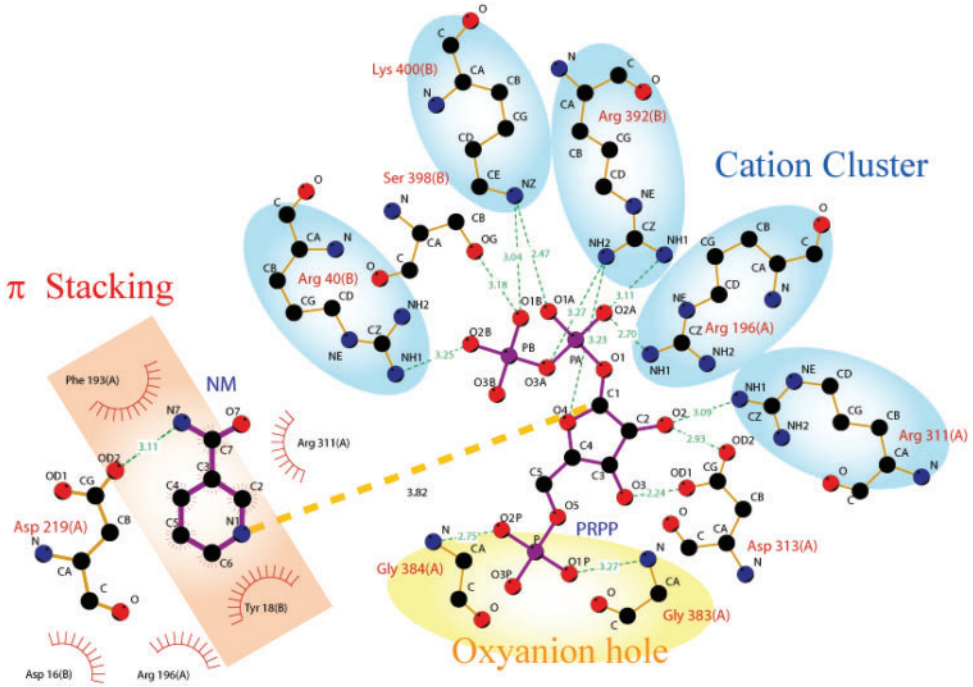

Fig. 8 The LIGPLOT of possible substrates-NMPRTase interactions. Atom labels: oxygen (red), nitrogen (blue), carbon (black) and phosphorus (purple).

Asp 313(A) (Fig. 8). The Pi group on C5′ forms hydrogen bonds with NHs of Gly 383(A) and Gly 384(A) to be involved in an oxyanion-hole-like pocket surrounded by the loop $Gly^{381}Ser^{382}Gly^{383}Gly^{384}Gly^{385}$, corresponding to the conserved loop motif of $h^{269}Ser^{270}Gly^{271}Gly^{272}h^{273}$ (h stands for a hydrophobic residue) in TaNAPRTase (*33*) and MtQAPRTase (*34*). The pyrophosphate (PPi) group on C1′ of PRPP is firmly bound to the enzyme through a network of hydrogen bonds and electrostatic interactions in a cationic cluster consisting of basic residues of Arg 40(B), Arg 196(A), Arg 392(B), Arg 311(A) and Lys 400(B) (Fig. 8). In addition to these interactions, there were several water molecules clearly located in the vicinity of NM (Fig. 5) and PRPP (Fig. 6). The effects of these bound water molecules are discussed in the following section.

Discussion

Reaction kinetics investigated by NMR and related to X-ray structures

To analyze the reaction of NMPRTase in the context of the suggested multifunctional character, it is indispensable to allow for a variety of regulatory effects caused by individual substances that could possibly be involved in the enzyme kinetics. However, the majority of methods for measuring the enzyme activity of NMPRTase have been limited to those determining the kinetic parameters by monitoring the concentration of NMN (or PRPP) indirectly (*15*, *16*), assuming that the rate-determining step of the whole system lies on the NMPRTase reaction, and that the enzymatic reaction proceeds without any interference due to the coexistence of the coupled enzyme system. It is thus desirable to use approaches not restricting the object to a single substrate or product. In fact, an impressive finding of the reversible nature of this enzyme reaction has been achieved by measuring the concentrations of radioactive NM and NMN simultaneously (*20*). This suggests that the reaction could be understood more comprehensively by taking into account every component involved. We employed the real-time monitoring of the concentration change with respect to 'all' the substrates and products (PRPP, NMN, NM and PPi) in ^{31}P and ^{1}H NMR spectra in a system containing NMPRTase as the sole enzyme. Eventually, ^{31}P and ^{1}H NMR measurements enabled us to monitor the decomposition of PPi to Pi and the formation of R-1,5-CP and 5PR-1,2-CP in addition to the concentration change of PRPP.

Owing to the apparently uncorrelated time-dependent changes between [NM] and [NMN] in the forward reaction, the ratio of [NMN]/[NM] did not converge into a constant value indicative of the existence of a certain equilibrium state. The convergence was observed only when we took the product of ratios [PPi]/[PRPP] and [NMN]/[NM] obtained from ^{31}P and ^{1}H NMR signal intensities, respectively, by assuming the equilibrium represented by equation (1b) (Fig. 3B). The resulting equilibrium constant $K = [NMN][PPi]/([NM][PRPP]) = 0.14$, was in agreement with the ratio of forward and backward reaction rate constants: $K = k_{2(1)}/k_{2(-1)} = 0.16$. Taking the ratios [PPi]/[PRPP] and [NMN]/[NM] based on ^{31}P and ^{1}H NMR signal intensities should minimize the error caused by the inherent difficulty in determining the absolute concentration of each component. In the backward reaction

starting from NMN and PPi, we obtained the equilibrium constant $K = [NMN][PPi]/([NM][PRPP]) = 0.18$, being almost the same value as that for the forward reaction (0.14) as expected from the reversibility of the reaction. Probably, the agreement of these equilibrium constants including the reported one (*20*) reflects the thermodynamic property of the system where the enzyme acts just as a catalyst that drives the reaction to approach a given equilibrium state. That is, the equilibrium constant is invariable with respect to the change of enzyme concentration or enzyme activity, which can be altered by a variety of possible inhibitory effects caused by substrates, products and byproducts. Therefore, the relatively small difference between the equilibrium constants is remarkable because the involvement of considerable error due to the contamination of PRPP with up to 10% of the impurities such as R-1,5-CP and 5PR-1,2-CP had been anticipated; these compounds can compete with PRPP or NMN for the binding site in both forward and backward reactions, interfering with the reaction to affect the rate constants $k_{2(1)}$ and $k_{2(-1)}$ differently.

The relationship between tertiary structure and the reaction mechanism

In both of these substitution reactions represented in equation (1a), there are two possibilities that the C1′ configuration of the ribose rings of PRPP and NMN is inverted: (i) the S_N1 mechanism in which PPi is released spontaneously to form the carbocation as the intermediate; and (ii) the S_N2 mechanism where the release of PPi occurs simultaneously with nucleophilic attack by the nitrogen atom of the pyridine ring (Scheme 1).

For the majority of glycosidases including enzymes that catalyze the substitution at the glycoside linkages, the plausible mechanism assumed is S_N1-type as exemplified in hen egg-white lysozyme (*36*). In the X-ray structures of these enzymes, a highly distorted half-chair conformation of the substrate sugar ring could be observed almost invariably, suggesting that considerable conformational strain is required for the formation of a planar structure around the sp^2-hybridized ribose-C1′ carbon of the carbocation intermediate (*37*). However, the presumed distortion of the ribose rings has not been recognized in the complexes of PRPP and NMN with NMPRTase; the 3′-exo conformation determined for the ribose ring in the enzyme-bound PRPP corresponds to one of the unconstrained structures of NMN in aqueous solution (*38*). If the carbocation intermediate exists, there should be at least one negatively charged group to stabilize the cationic intermediate by forming an ion pair. Although the carboxyl group of Asp 313 is the most plausible candidate for stabilizing positive charge in the ribose moieties of NMN (*15–17*) and PRPP, it is not close enough to be able to interact with O4′ of the ribose ring but more likely to interact with the C2′ and C3′-hydroxyl groups of the ribose ring (Fig. 6). The negative charge of the Pi group at the ring C5′ position of NMN or PRPP appears to be replaceable with that of Asp 313. However, a network of hydrogen bonds within the loop, $Gly^{381}Ser^{382}Gly^{383}Gly^{384}Gly^{385}$ (Fig. 8), keeps the Pi group away from the C1′ atom and disperses the negative charge. Although some authors have attributed the requisite negative charge to the phosphoryl group considered to modify His 247 (*15*, *19*), the distance between the C1′ carbon and the

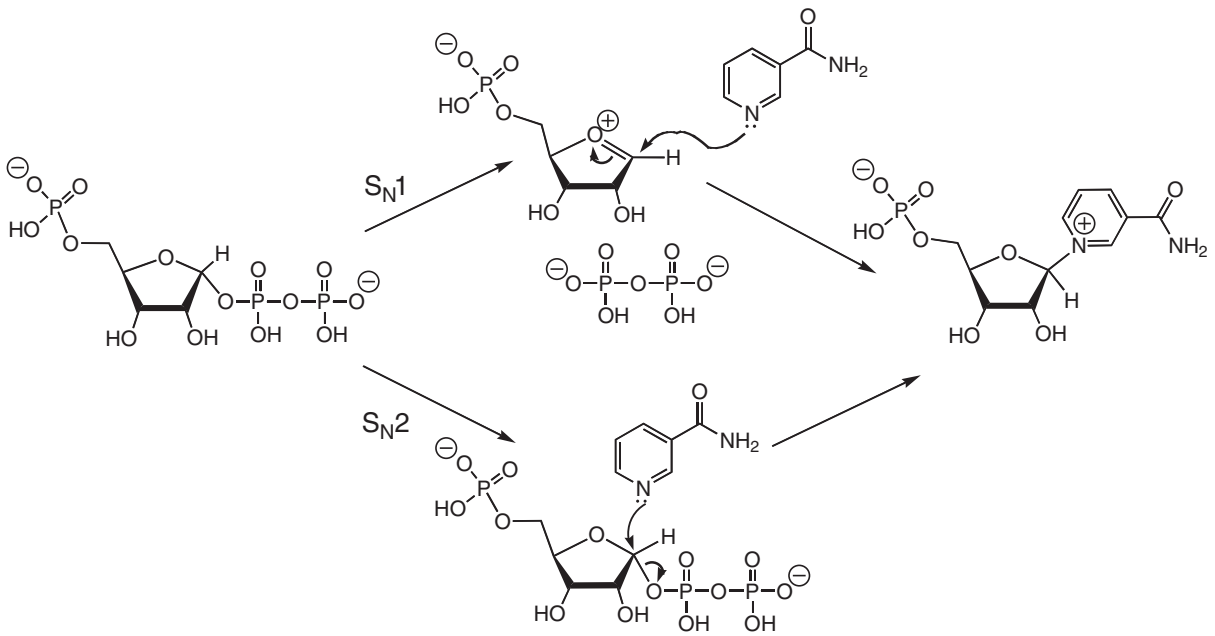

Scheme 1 Two possible reaction mechanisms of NMPRTase catalysis. The pyrophosphate group of PRPP is substituted by NM, which acts as a nucleophile. In the S_N1 mechanism (upper route), the pyrophosphate group spontaneously leaves from the C1′ carbon of sugar ring, creating the intermediate ribo-oxocarbocation. In the S_N2 mechanism (lower route), nucleophilic attack of NM is required to release the pyrophosphate group. Note that the arrows indicate the direction of the forward reaction but that the direction can be reverted to describe the backward reaction.

fluorine atom of BeF_3, which mimics the Pi moiety of phosphohistidine, is at least 4.0 Å, providing only weak electrostatic stabilization of the cationic intermediate (*19*). A cation-π interaction proposed to occur between the carbocation intermediate and Tyr 118 in hypoxanthine-guanine phosphoribosyltransferase (HGPRT) (*39*) might not apply to NMPRTase, because Tyr 18(B) corresponding to Tyr 118 in HGPRT is not located appropriately. In summary, there is no positive evidence for the existence of a carbocation intermediate supportive of an S_N1 mechanism in the present experiments on NMPRTase.

Owing to essentially identical structures of NMPRTase and its complexes with NM, NMN and PRPP, we could assume a model that describes the spatial arrangements of these substrates and product during the reaction. The distance between the nucleophilic nitrogen atom (N1) of NM and C1′ of PRPP was estimated to be 3.82 Å (Fig. 8), which could be shortened by 2.18 Å due to the conformational change of the ribose ring from the C3′-exo of PRPP to C3′-endo of NMN (Fig. 7). This signifies that only the conformational change of the ribose ring of PRPP is necessary to undergo the substitution reaction. With the shorter distance between the reactants, NM can attack the ribose C1′-carbon atom from the opposite position to the O1′-oxygen atom of the PPi group in the manner of an S_N2 reaction. The alignment of the nucleophile and the leaving group (NM and PPi, respectively, in the forward reaction) facilitates the requisite inversion of configuration at the C1′ carbon of the ribose ring as illustrated in Fig. 7. This geometry of reactants and products is consistent with the suggested migration of the ribosyl anomeric carbon in reaction coordinate motion (*19*). Note that such a mechanism does not require the formation of an explicit cationic intermediate but proceed in accord with the principle of least nuclear motion (*40*, *41*). More importantly, a revised mechanism of hen egg-white lysozyme catalysis involves the formation of a covalent intermediate, which is not a carbocation, and the electrophilic migration of the ribose C1′ carbon along the reaction coordinate (*41*).

The catalytic activity of the enzyme has been reported to be $k_{cat} = 2.0 \times 10^{-2}$/s (*42*), which is too slow to avoid causing the possible hydrolytic degradation of NMN or PRPP to 5′-phosphoribose (5PR), unless NMPRTase possesses a structure that could efficiently shield the active site from mobile water molecule(s) like some PRTases (*43–45*). Because there are at least four water molecules within 5 Å from the C1′ carbon of the enzyme-bound PRPP in the active site (Fig. 6), it is unlikely to assume the requisite waterproof structure in NMPRTase. This casts doubt on the existence of the carbocation intermediate, which is so unstable in aqueous media that it decomposes to 5PR at a rate as fast as 10^{12}/s (*46*), which is much faster than the observed rate of an ordinary substitution reaction. In the catalysis of CD38, which is also a multi-functional enzyme possessing NAD^+ cyclase activity, 5PR does arise from NMN, probably owing to the lack of such a waterproof structure in the active site, allowing a cationic intermediate to exist (*47*, *48*). Conversely, it is reasonable that the reaction of hypoxanthine PRTase from *Trypanosoma cruzi* has been described to proceed in the S_N2-type mechanism, because of the finding of an intact PRPP (substrate) at the active site in which the access of water is not structurally excluded (*49*). In this respect, the resistance of PRPP and NMN to the attack of water in NMPRTase is compatible with the S_N2 mechanism, in which the nucleophilicity of water molecule is distinctively much lower than that of pyridine-ring nitrogen and PPi anion by several orders of magnitude in ordinary solution [Tables 2.6 and 4.3 in Ref. (*50*)].

Although KIEs could be the more reliable criteria to distinguish between S_N1 and S_N2 mechanisms, the reversibility of the reaction [equation (1a)] imposes great difficulties on the determination of intrinsic KIE values due to the involvement of both forward and reverse reactions (*51*). This fact, along with the difficulty in obtaining KIEs with the more accurate measurement of reaction rates in this isolated enzyme system, prevented us from applying this technique.

Function of NMPRTase inferred from its structure and mechanism

The fact that NMPRTase in the free and substrate-bound states had almost indistinguishable structure showed a close resemblance to APRTase where the adenine ring and the 5′-ribosyl Pi group remain fixed during the enzyme reaction while the ribosyl anomeric carbon exhibits only a slight excursion (*35*). Based on the stereochemistry of the S_N2 mechanism, we consider that the role of NMPRTase is to provide a nucleophile (NM or PPi) and a phosphoribose (PRPP or NMN) with sites for attacking and being attacked, respectively, at precisely the opposite position with respect to the C1′ atom. The activation of water molecule for the false attack on the C1′ atom of bound substrate is probably prevented by the highly cationic environment in the active site. The advantage of catalyzing the reaction without forming a highly unstable carbocation is that the enzyme could exclude PRPP and NMN from their decomposition to 5PR, thus securing the integrity of the metabolic pathways such as NAD-biosynthesis. This property contrasts with those of hydrolytic PRTases such as 5′-methylthioadenosine/*S*-adenosyl homocysteine nucleosidase, many of which catalyze the reaction via the S_N1 mechanism as judged from the KIE values (*52*).

Concerning the effect of the anti-cancer drug FK866 on NMPRTase, the suggested mode of inhibition was inconsistent, whether it is competitive (*16*) or non-competitive (*7*), based on the kinetics of the enzyme reaction. Judged from almost the same structure of NMPRTase in the complex with FK866 as that with NMN (*7*) without any appreciable conformational distortion, FK866 might not inhibit the enzyme as a transition-state analogue or a mimic of the carbocation but just as a structural analogue of both NM and NMN. It is therefore reasonable to think of FK866 as a competitive inhibitor sharing the single binding site with the genuine substrate. This reminds us of the inhibition of Goldi α-mannosidase II with mannostatin A, which has proved to bind with the enzyme not

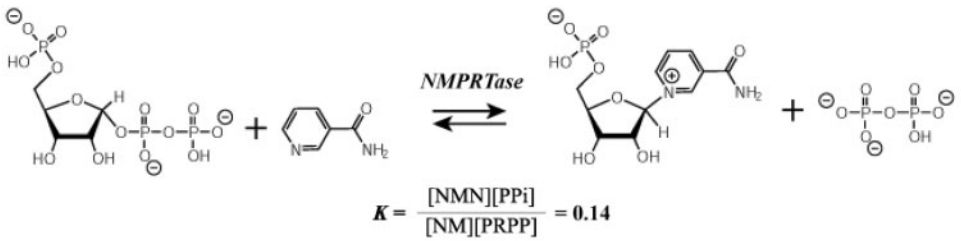

Fig. 9 The preference of NMPRTase catalysis for the backward reaction is characterized by a low equilibrium constant of 0.14. Note that NM can be recycled from NMN without the need of decomposing NAD (see Fig. 1 for comparison).

by mimicking a ribocarbocation-like intermediate but by the covalently linked mannosyl intermediate (*53*). Accordingly, this enzyme could possibly be inhibited effectively by making the reaction irreversible either with a structural analogue of NMN or PRPP modified to bind strongly to the enzyme or with a mimic of NM or PPi with higher nucleophilicity. The physiological effects of such an inhibitor should therefore be accessed with some caution in connection with the reversible nature of this enzyme.

The preference of the equilibrium to the left-hand side of equation (1a) implies that NMPRTase can act as an enzyme responsible for maintaining a high-physiological level of NM at the cost of NMN rather than for producing NMN at the first step of NAD-biosynthesis. Although enzymes such as CD38 and sirtuins also produce NM by degrading NAD (*42*, *48*, *49*), NMPRTase is distinguished from other NAD-consuming enzymes by its ability to maintain the concentrations of NM, NMN and PRPP at certain physiological levels dictated by the equilibrium constant (0.14–0.16). Owing to this equilibrium, a complete or extreme depletion of any one of these components, each of which has its own biological significance, is avoided. Because the composition of the equilibrium mixture depends on the concentrations of PRPP and PPi as well as those of NM and NMN, it is possible to drive the reaction in any direction. For example, production of NMN is enhanced if the co-product PPi is consumed rapidly even when the concentration of NM is lower than the normal level of 0.4–0.5 μM in human serum (*54*). It has been reported that the equilibrium point was shifted dramatically by the addition of ATP, assuming an energy coupling, which involves the covalent modification of His 247 associated with the ATPase activity of NMPRTase (*20*). Although the detailed mechanism of ATP reaction remains to be elaborated, it is also possible to interpret the shift of equilibrium point by assuming a newly established equilibrium consisting of ATP as one of the components explicitly included in the equilibrium constant, which might differ from $K = [NMN][PPi]/([NM][PRPP])$. Considering the versatility of NMPRTase activity in response to the composition of an equilibrium mixture, we expect to soon understand the multi-functional property of NMPRTase, which can create a wide variety of conditions in different organs or between inside and outside of cells (*55*).

One of the main features of the present study is that the reaction of NMPRTase is reversible to attain an equilibrium in favor of the formation of PRPP with consumption of NMN and PPi as represented by the equilibrium constant $K = [NMN][PPi]/([NM][PRPP]) = 0.14$, which is in good agreement with the corresponding value 0.16 obtained from the ratio of second-order rate constants for forward and backward reactions, or $k_{2(1)}/k_{2(-1)}$. The agreement in these values of equilibrium constant is possible only when the rates of forward and backward reactions are balanced at the equilibrium state as expressed by the equation $k_{2(1)}[NM][PRPP] = k_{2(-1)}[NMN][PPi]$, which derives from equation (1b). The preference for the backward reaction to the direction opposite to the ordinary catalytic process could allow NMPRTase to exhibit an additional function such as the maintenance of a high-physiological level of NM at the expense of NMN (Fig. 9). The X-ray crystallography of NMPRTase revealed that the active-site structure accommodates PPi and NM as nucleophiles for the substitution reaction effectively discriminating against water molecules, which could otherwise hydrolyze PRPP and NMN if the reaction is to proceed in the manner of S_N1 mechanism. These features of the structure and reaction mechanism would pave the way for further study of catalysis, regulation and multi-functional behaviour of NMPRTase.

Supplementary data

Supplementary data are available at *JB* online.

Acknowledgements

The authors thank Prof. I. Shimomura and Dr A. Fukuhara (School of Medicine, Osaka University) for the generous gift of the recombinant gene of human NMPRTase. They also thank Dr K. Hasegawa and Dr H. Sakai of Japan Synchrotron Radiation Research Institute (JASRI) for their help during data collection. They also thank the organizing committee of SPring-8 for the approval of our proposal of the X-ray data collection (No. 2006A1719-NL-np-P3k).

Conflict of interest

None declared.

References

1. Katoh, A. and Hashimoto, T. (2004) Molecular biology of pyridine nucleotide and nicotine biosynthesis. *Front. Biosci.* **9**, 1577–1586

2. Magni, G., Amici, A., Emanuelli, M., Orsomando, G., Raffaelli, N., and Ruggieri, S. (2004) Enzymology of NAD^+ homeostasis in man. *Cell Mol. Life Sci.* **61**, 19–34
3. Voet, D. and Voet, J. G. (1995) *Biochemistry*. 2nd edn, J. Wiley & Sons, New York
4. Guse, A.H., Silva, C.P., Weber, K., Ashamu, G.A., Potter, B.V., and Mayr, G.W. (1996) Regulation of cADP-ribose-induced Ca^{2+} release by Mg^{2+} and inorganic phosphate. *J. Biol. Chem.* **271**, 23946–23953
5. Ziegler, M. (2000) New functions of a long-known molecule. Emerging roles of NAD in cellular signaling. *Eur. J. Biochem.* **267**, 1550–1564
6. Zerez, C.R., Roth, E.F. Jr, Schulman, S., and Tanaka, K.R. (1990) Increased nicotinamide adenine dinucleotide content and synthesis in *Plasmodium falciparum*-infected human erythrocytes. *Blood* **75**, 1705–1710
7. Hasmann, M. and Schemainda, I. (2003) FK866, a highly specific noncompetitive inhibitor of nicotinamide phosphoribosyltransferase, represents a novel mechanism for induction of tumor cell apoptosis. *Cancer Res.* **63**, 7436–7442
8. Drevs, J., Loser, R., Rattel, B., and Esser, N. (2003) Antiangiogenic potency of FK866/K22.175, a new inhibitor of intracellular NAD biosynthesis, in murine renal cell carcinoma. *Anticancer Res.* **23**, 4853–4858
9. Samal, B., Sun, Y., Stearns, G., Xie, C., Suggs, S., and McNiece, I. (1994) Cloning and characterization of the cDNA encoding a novel human pre-B-cell colony-enhancing factor. *Mol. Cell Biol.* **14**, 1431–1437
10. Rongvaux, A., Shea, R.J., Mulks, M.H., Gigot, D., Urbain, J., Leo, O., and Andris, F. (2002) Pre-B-cell colony-enhancing factor, whose expression is up-regulated in activated lymphocytes, is a nicotinamide phosphoribosyltransferase, a cytosolic enzyme involved in NAD biosynthesis. *Eur. J. Immunol.* **32**, 3225–3234
11. Segawa, K., Fukuhara, A., Hosogai, N., Morita, K., Okuno, Y., Tanaka, M., Nakagawa, Y., Kihara, S., Funahashi, T., Komuro, R., Matsuda, M., and Shimomura, I. (2006) Visfatin in adipocytes is upregulated by hypoxia through HIF1alpha-dependent mechanism. *Biochem. Biophys. Res. Commun.* **349**, 875–882
12. Tanaka, M., Nozaki, M., Fukuhara, A., Segawa, K., Aoki, N., Matsuda, M., Komuro, R., and Shimomura, I. (2007) Visfatin is released from 3T3-L1 adipocytes via a non-classical pathway. *Biochem. Biophys. Res. Commun.* **359**, 194–201
13. Hug, C. and Lodish, H.F. (2005) Medicine. Visfatin: a new adipokine. *Science* **307**, 366–367
14. Matsuzawa, Y. (2005) Adipocytokines and metabolic syndrome. *Semin. Vasc. Med.* **5**, 34–39
15. Wang, T., Zhang, X., Bheda, P., Revollo, J.R., Imai, S., and Wolberger, C. (2006) Structure of Nampt/PBEF/visfatin, a mammalian NAD^+ biosynthetic enzyme. *Nat. Struct. Mol. Biol.* **13**, 661–662
16. Khan, J.A., Tao, X., and Tong, L. (2006) Molecular basis for the inhibition of human NMPRTase, a novel target for anticancer agents. *Nat. Struct. Mol. Biol.* **13**, 582–588
17. Kim, M.K., Lee, J.H., Kim, H., Park, S.J., Kim, S.H., Kang, G.B., Lee, Y.S., Kim, J.B., Kim, K.K., Suh, S.W., and Eom, S.H. (2006) Crystal structure of visfatin/pre-B cell colony-enhancing factor 1/nicotinamide phosphoribosyltransferase, free and in complex with the anticancer agent FK-866. *J. Mol. Biol.* **362**, 66–77
18. Takahashi, R., Nakamura, S., Yoshida, T., Kobayashi, Y., and Ohkubo, T. (2007) Crystallization of human nicotinamide phosphoribosyltransferase. *Acta Crystallogr. Sect. F Struct. Biol. Cryst. Commun.* **63**, 375–377
19. Burgos, E.S., Ho, M.C., Almo, S.C., and Schramm, V.L. (2009) A phosphoenzyme mimic, overlapping catalytic sites and reaction coordinate motion for human NAMPT. *Proc. Natl Acad. Sci. USA* **106**, 13748–13753
20. Burgos, E.S. and Schramm, V.L. (2008) Weak coupling of ATP hydrolysis to the chemical equilibrium of human nicotinamide phosphoribosyltransferase. *Biochemistry* **47**, 11086–11096
21. Smbrook, J. and Russell, D.W. (2001) *Molecular Cloning: A Laboratory Manual*. 3rd edn, Cold Spring Harbor Laboratory Press, New York
22. Press, W.H., Teukolsky, S.A., Vettring, W.T., and Flannery, B.P. (1992) *Numerical Recipes*, Cambridge University Press, Cambridge, UK
23. Otwinowski, Z. and Minor, W. (1997) Processing of X-ray diffraction data collected in oscillation mode. *Methods Enzymol.* **276**, 307–326
24. Collaborative Computational Project, No. 4. (1994) The CCP4 suite: programs for protein crystallography. *Acta Crystallogr. D Biol. Crystallogr.* **50**, 760–763
25. Vagin, A. and Teplyakov, A. (1997) MOLREP: an automated program for molecular replacement. *J. Appl. Cryst.* **30**, 1022–1025
26. Murshudov, G.N., Vagin, A.A., Lebedev, A., Wilson, K.S., and Dodson, E.J. (1999) Efficient anisotropic refinement of macromolecular structures using FFT. *Acta Crystallogr. D Biol. Crystallogr.* **55**, 247–255
27. McRee, D.E. (1999) XtalView/Xfit–A versatile program for manipulating atomic coordinates and electron density. *J. Struct. Biol.* **125**, 156–165
28. Lamzin, V.S. and Wilson, K.S. (1993) Automated refinement of protein models. *Acta. Crystallogr. D Biol. Crystallogr.* **49**, 129–147
29. Laskowski, R.A., MacArthur, M.W., Moss, D.S., and Thornton, J.M. (1993) PROCHECK: a program to check the stereochemical quality of protein structures. *J. Appl. Cryst.* **26**, 283–291
30. Wallace, A.C., Laskowski, R.A., and Thornton, J.M. (1995) LIGPLOT: a program to generate schematic diagrams of protein-ligand interactions. *Protein Eng.* **8**, 127–134
31. Trembacz, H. and Jezewska, M.M. (1990) The route of non-enzymic and enzymic breakdown of 5-phosphoribosyl 1-pyrophosphate to ribose 1-phosphate. *Biochem. J.* **271**, 621–625
32. Dennis, A.L., Puskas, M., Stasaitis, S., and Sandwick, R.K. (2000) The formation of a 1-5 phosphodiester linkage in the spontaneous breakdown of 5-phosphoribosyl-α-1-pyrophosphate. *J. Inorg. Biochem.* **81**, 73–80
33. Shin, D.H., Oganesyan, N., Jancarik, J., Yokota, H., Kim, R., and Kim, S.H. (2005) Crystal structure of a nicotinate phosphoribosyltransferase from *Thermoplasma acidophilum*. *J. Biol. Chem.* **280**, 18326–18335
34. Sharma, V., Grubmeyer, C., and Sacchettini, J.C. (1998) Crystal structure of quinolinic acid phosphoribosyltransferase from *Mycobacterium tuberculosis*: a potential TB drug target. *Structure* **6**, 1587–1599
35. Shi, W., Sarver, A.E., Wang, C.C., Tanaka, K.S., Almo, S.C., and Schramm, V.L. (2002) Closed site complexes of adenine phosphoribosyltransferase from *Giardia lamblia* reveal a mechanism of ribosyl migration. *J. Biol. Chem.* **277**, 39981–39988
36. Strynadka, N.C. and James, M.N. (1991) Lysozyme revisited: crystallographic evidence for distortion of an

N-acetylmuramic acid residue bound in site D. *J. Mol. Biol.* **220**, 401–424
37. Craig, S.P. 3rd and Eakin, A.E. (2000) Purine phosphoribosyltransferases. *J. Biol. Chem.* **275**, 20231–20234
38. Oppenheimer, N.J. and Kaplan, N.O. (1976) Proton magnetic resonance study of the intramolecular association and conformation of the alpha and beta pyridine mononucleotides and nucleosides. *Biochemistry* **15**, 3981–3989
39. Heroux, A., White, E.L., Ross, L.J., Kuzin, A.P., and Borhani, D.W. (2000) Substrate deformation in a hypoxanthine-guanine phosphoribosyltransferase ternary complex: the structural basis for catalysis. *Structure* **8**, 1309–1318
40. Hine, J. (1978) The principle of least nuclear motion. *Adv. Phys. Org. Chem.* **15**, 1–61
41. Vocadlo, D.J., Davies, G.J., Laine, R., and Withers, S.G. (2001) Catalysis by hen egg-white lysozyme proceeds via a covalent intermediate. *Nature* **412**, 835–838
42. Revollo, J.R., Grimm, A.A., and Imai, S. (2004) The NAD biosynthesis pathway mediated by nicotinamide phosphoribosyltransferase regulates Sir2 activity in mammalian cells. *J. Biol. Chem.* **279**, 50754–50763
43. McClard, R.W., Fischer, A.C., Mauldin, S.K., and Jones, M.E. (1984) 5-Phosphorylribose 1-α-methylenebisphosphonate: Properties of a substrate analog of 5-phosphorylribose 1-α-diphosphate. *Bioorg. Chem.* **12**, 339–348
44. Krahn, J.M., Kim, J.H., Burns, M.R., Parry, R.J., Zalkin, H., and Smith, J.L. (1997) Coupled formation of an amidotransferase interdomain ammonia channel and a phosphoribosyltransferase active site. *Biochemistry* **36**, 11061–11068
45. Fedorov, A., Shi, W., Kicska, G., Fedorov, E., Tyler, P.C., Furneaux, R.H., Hanson, J.C., Gainsford, G.J., Larese, J.Z., Schramm, V.L., and Almo, S.C. (2001) Transition state structure of purine nucleoside phosphorylase and principles of atomic motion in enzymatic catalysis. *Biochemistry* **40**, 853–860
46. Amyes, T.L. and Jencks, W.P. (1989) Lifetimes of oxocarbenium ions in aqueous solution from common ion inhibition of the solvolysis of α-azido ethers by added azide ion. *J. Am. Chem. Soc.* **111**, 7888–8900
47. Sauve, A.A., Munshi, C., Lee, H.C., and Schramm, V.L. (1998) The reaction mechanism for CD38. A single intermediate is responsible for cyclization, hydrolysis, and base-exchange chemistries. *Biochemistry* **37**, 13239–13249
48. Sauve, A.A., Wolberger, C., Schramm, V.L., and Boeke, J.D. (2006) The biochemistry of sirtuins. *Annu. Rev. Biochem.* **75**, 435–465
49. Focia, P.J., Craig, S.P. 3rd, and Eakin, A.E. (1998) Approaching the transition state in the crystal structure of a phosphoribosyltransferase. *Biochemistry* **37**, 17120–17127
50. Fersht, A. (1999) *Structure and Mechanism in Protein Science: A Guide to Enzyme Catalysis and Protein Folding*. W.H. Freeman, New York
51. Northrop, D.B. (1981) The expression of isotope effects on enzyme-catalyzed reactions. *Ann. Rev. Biochem.* **50**, 103–131
52. Singh, V., Lee, J.E., Nunez, S., Howell, P.L., and Schramm, V.L. (2005) Transition state structure of 5′-methylthioadenosine/S-adenosylhomocysteine nucleosidase from *Escherichia coli* and its similarity to transition state analogues. *Biochemistry* **44**, 11647–11659
53. Kawatkar, S.P., Kuntz, D.A., Woods, R.J., Rose, D.R., and Boons, G.J. (2006) Structural basis of the inhibition of Golgi alpha-mannosidase II by mannostatin A and the role of the thiomethyl moiety in ligand-protein interactions. *J. Am. Chem. Soc.* **128**, 8310–8319
54. Bernofsky, C. (1980) Physiology aspects of pyridine nucleotide regulation in mammals. *Mol. Cell Biochem.* **33**, 135–143
55. Belenky, P., Bogan, K.L., and Brenner, C. (2007) NAD^+ metabolism in health and disease. *Trends Biochem. Sci.* **32**, 12–19